Article:
Smith, CC, Paton, JFR, Chakrabarty, S orcid.org/0000-0002-4389-8290 et al. (1 more author) (2017) Descending systems direct development of key spinal motor circuits. Journal of Neuroscience, 37 (26). pp. 6372-6387. ISSN 0270-6474

https://doi.org/10.1523/JNEUROSCI.0149-17.2017

Descending systems direct development of key spinal motor circuits

Abbreviated title: Postnatal development of spinal motor circuits

Calvin C. Smith *[1], Julian F.R. Paton[2], Samit Chakrabarty[1], Ronaldo M. Ichiyama*[1]

[1]School of Biomedical Sciences, University of Leeds, Leeds, United Kingdom, LS2 9JT

[2]Department of Physiology, School of Medical Sciences, University of Bristol, Bristol, United Kingdom, BS8 1TH

*Corresponding author

email: calvin.smith@ucl.ac.uk

Pages: 38

Figures:10 Tables:1

Abstract words: 175

Significance statement words:116

Introduction words:645

Discussion words:1530

Conflicts of interest: The authors declare no competing financial interests.

Abstract

The formation of mature spinal motor circuits is dependent on both activity dependent and independent mechanisms during postnatal development. During this time, reorganisation and refinement of spinal sensorimotor circuits occurs as supraspinal projections are integrated. However, specific features of postnatal spinal circuit development remain poorly understood. This study provides the first detailed characterisation of rat spinal sensorimotor circuit development in the presence and absence of descending systems. We show that development of proprioceptive afferent (PA) input to motoneurones (MN) and Renshaw cells (RC) is disrupted by thoracic spinal cord transection (TX) at postnatal day 5 (PN5). PN5TX also lead to malformation of GABApre neuron axo-axonic contacts on Ia afferents and the recurrent inhibitory circuit between MN and RC. Using a novel in situ perfused preparation for studying motor control, we show that malformation of these spinal circuits leads to hyperexcitability of the monosynaptic reflex. Our results demonstrate that removing descending input severely disrupts development of spinal circuits and identifies key mechanisms contributing to motor dysfunction in conditions such as cerebral palsy and spinal cord injury.

Significance statement

Acquisition of mature behaviour during postnatal development correlates with arrival and maturation of supraspinal projections to the spinal cord. However, we know little about the role descending systems play in maturation of spinal circuits. Here, we characterise postnatal development of key spinal microcircuits in the presence and absence of descending systems. We show

that formation of these circuits is abnormal following early (PN5) removal of descending systems, inducing hyperexcitability of the monosynaptic reflex. The study is a detailed characterisation of spinal circuit development elucidating how these mechanisms contribute to motor dysfunction in conditions such as cerebral palsy and spinal cord injury. Understanding these circuits is crucial to develop new and improve current therapeutics in such conditions.

Introduction

In most mammals, mature over ground locomotion is acquired throughout postnatal development, despite the early emergence of functioning brainstem and spinal locomotor circuits (Cazalets et al., 1990; Van Hartesveldt et al., 1991; Ozaki et al., 1996). In rats for example, quadrupedal locomotion is achieved at postnatal day (PN) 10-12, with a striking transition to motor-maturity occurring at PN14 (Altman & Sudarshan, 1975). By PN21, locomotion is indistinguishable from that of adult animals. This protracted acquisition of over ground locomotion is thought to reflect activity dependent mechanisms of motor circuit development as the animal begins to interact with its environment. For example, corticospinal tract (CST) terminations only reach the grey matter of caudal spinal segments at PN9-10, with innervation patterns maturing by PN14, the same time as locomotion (Donatelle, 1977). Brainstem structures reach the lumbar spinal cord at or shortly after birth, but also undergo significant development during the first 2 weeks (Bregman, 1987; Brocard et al., 1999; Vinay et al., 2005)

Conversely, sensory systems make functional connections with their spinal targets prenatally, with reorganisation and refinement taking place PN (Fitzgerald, 2005; Chakrabarty & Martin, 2011a). Proprioceptive Ia afferents

(PA) form functional monosynaptic connections with homonymous and synergistic motoneurones (MNs) at embryonic day 19 (E19) (Kudo & Yamada, 1985; Chen et al., 2003). This sensory-motor connectivity exhibits stringent specificity that is mainly dependent upon MN positional cues and cell surface signalling (Mears & Frank, 1997; Sürmeli et al., 2011; Fukuhara et al., 2013). Whilst features such as sensory-motor fidelity appear hardwired, postnatal retraction of dense PA projections in the cervical cord is thought to depend on late integration of descending systems (Gibson & Clowry, 1999; Chakrabarty & Martin, 2011a). This profile has never been demonstrated in the lumbar spinal cord however, despite obvious functional differences, especially in fine motor control.

Functional outcomes following neonatal injuries to descending systems underline the importance of supraspinal projections to spinal sensorimotor circuit development. In cerebral palsy (CP), perinatal insults to the brain lead to debilitating spasticity resulting from aberrant growth and reduced modulation of sensory afferents (Dietz & Sinkjaer, 2007; Rosenbaum et al., 2014). Interestingly, sensory afferents also contribute to the remarkable recovery of locomotion seen following neonatal spinal transection in rodents (Weber & Stelzner, 1977; Commissiong & Toffano, 1989; Saunders et al., 1998; Petruska et al., 2007; Tillakaratne et al., 2010; Ichiyama et al., 2011). With locomotor training, prospects of functional recovery in neonatally transected animals far outweigh those of adult transected animals, suggesting spinal circuits in the **former** are better able to utilise sensory information in the absence of supraspinal control. Indeed, although sensory afferents are important to recovery, Bui et al. (2016) show that an interposed sensorimotor microcircuit become indispensable following adult spinal TX. It is vital therefore, that we

further understand the development of spinal sensorimotor circuits in normal and injured states.

Recently, important steps have been taken towards understanding development of specific spinal circuits. Siembab et al. (2016) genetically manipulated PA inputs in mice to demonstrate that maturation of motor axon inputs to RC is dependent upon the strength of PA input during early PN development. Additionally, Mendelsohn et al. (2015) showed that genetically blocking neurotransmission between PA and MN during development leads to increased incidence of PA projections to heteronymous (synergist) MNs.

In this study, we provide the first detailed characterisation of spinal sensorimotor circuit development in the presence and absence of descending systems. We show that normal development of PA input to all regions of the spinal cord, including MN and RCs is disrupted following neonatal transection. This leads to malformation of microcircuits involved in recurrent inhibition of MNs and presynaptic inhibition of afferents. We used an in situ, perfused whole rat preparation to study physiological development of spinal motor circuits and show that a lack of descending input and resultant malformation of inhibitory microcircuits resulted in hyperexcitability of the monosynaptic reflex (MSR).

Materials and Methods

Experiments and procedures were performed in a manner that conformed to the UK Home Office guidelines regarding the use of animals. Approval was granted by the local ethics committee (University of Leeds).

Animals

Wistar rats, both male and female were used for all experiments. The ages of assessment for both intact and TX rats were PN10, PN14 and PN21. These ages were used because they represent significant behavioural milestones based on previous literature (Altman & Sudarshan, 1975; Westerga & Gramsbergen, 1993a; Westerga & Gramsbergen, 1993b). For example, at PN10 (immature time point) rats are capable of some quadrupedal weight bearing but locomotor abilities are minimal. At PN14 (transition time point) there is a striking transition to adult-like locomotion with some deficits in speed and accuracy. At PN21 (mature time point) over ground locomotor kinematics are indistinguishable from the adults.

Decerebrate perfused rat preparation

Preparation Set up

Wistar rats aged 10-21 days PN were weighed then anaesthetised with Isoflurane (95%0_2, 5% CO_2 mix, 5% induction, 2% maintenance) until loss of paw withdrawal. A midline laparotomy was performed and the stomach, spleen and free intestine were ligated and removed. Once evisceration was complete, the animal was transferred to an ice bath containing artificial cerebrospinal fluid (ACSF composition listed below) bubbled with carbogen gas (95%O_2, 5% CO_2) and a pre-collicular decerebration was performed and the skin removed. The animal was then transferred to a cold dissecting dish (ACSF, < 3℃), where a midline sternotomy permitted access to the chest cavity. Most of the lung parenchyma and thymus were removed for easy access to the heart. An incision was made into the apex of the heart for later insertion of the cannula (Ø 1.25 mm, DLR-4, Braintree Scientific, MA, USA) before another small incision was made into the right atrium to allow draining of the perfusate. The animal

was then transferred to the recording chamber and rested (supine) on a custom sylgard (Dow Corning) bed. The cannula was immediately inserted transcardially into the ascending aorta (Figure 1A). The cannula was fixed in place using a single suture (no 2, silk, MERSILK). Once the cannula was secured the animal was carefully transferred to the prone position and the flow rate was increased gradually over 1 minute until further increases in flow failed to increase pressure (~40 mmHg). The pressure before and after turning the animal were compared to ensure the cannula had not retracted from the aorta. The oxygenated perfusate was pumped from a flask to the preparation via a heat exchanger (32°C), bubble traps and a particle filter (25μm screen, Millipore) (Figure 1B). The flow was generated by a pump (Gilson Minipuls 3) with the volume maintained at 200 mL. After initiation of flow, the heart resumed beating immediately and the preparation started to warm up. Successful perfusion was indicated by liver blanching, filling of the scull cavity, atrial distension and spontaneous motor activity. 100-200 pM vasopressin (Arg-8-Vasopressin, AVP, AbcamBiochemicals) was added to the perfusate to increase the systemic resistance and pressure to 50-80 mmHg which has been deemed sufficient for adequate perfusion of the caudal spinal cord (Pickering & Paton, 2006). Respiratory contractions were observed once the pressure reached 40-50 mmHg, indicating brainstem viability (Figure 2A-C). Lumbar spinal cord viability was initially observed by spontaneous rhythmic hind limb movements and nociceptive reflexes in response to tail and hind limb pinches (Figure 2D-E). Once stimulation and recording equipment were in place, robust H reflex responses confirmed viability of the lumbar cord.

Solutions

Modified Ringers solution (ACSF) was made up of: (mM) NaCl (125); $NaHCO_3$ (25); KCL (3); $CaCl_2$ (2.5); $MgSO_4$ (1.25); KH_2PO_4 (1.25); D-Glucose (10). A PH of 7.35-7.4 was attained once carbogenated. Polyethylene glycol (1.25%) was added as an oncotic agent.

H reflex

Isolation of nerve

Once the cannula was secure and the animal was fixed in place using ear bars, a small incision was made into the fascia separating the quadriceps and hamstring muscles. Using blunt dissection, the muscles were reflected, the sciatic nerve carefully freed from surrounding tissue (apart from its insertion into gastrocnemius) and tibial nerve located and mounted on a bipolar hook electrode (Figure 3D).

Stimulation and Recording Methods

The nerve was stimulated via hook electrodes with a monophasic square pulse generated by an ISO-Flex isolated stimulator. Square pulses (0.3ms) were generated every 3 seconds using the A.M.P.I Master-8 to trigger the stimulator, allowing 5s recovery between pulses. Evoked intramuscular responses were recorded using fine bipolar needle electrodes (SpesMedica) inserted into the gastrocnemius muscle. For each animal, graded stimulation of the nerve produced a recruitment curve which was used to determine Ia afferent and motor axon thresholds (Figure 3A-C). H reflex threshold was determined as the intensity at which the smallest visible response occurred at a frequency of 50%. H reflexes on the ascending portion of the recruitment curve (small M wave, large H wave) were deemed optimal for paired pulse analysis. At the end of the experiment to further verify the H reflex, an axotomy was performed by

severing the nerve between the hook electrode and the exit of the mixed sciatic nerve from the spinal cord (Figure 3D). This severed the sensory and motor nerves to and from the spinal cord but retained the motor axons between the hook and recording electrodes. Axotomy demonstrated that the H reflex was abolished but a strong M wave was retained (Figure 3E).

Paired pulse stimulation was used to assess excitability of the central circuits by evaluating the H reflex and its modulation. Dual pulses were administered to the nerve at intervals ranging from 1-700ms and the level of depression was calculated to produce a depression curve. At least 15 traces were recorded for each interval tested and there was a minimum rest period of 1 minute between trials. Control (single pulse) trials, also consisting of 15 traces, preceded each test trial for direct comparison and normalisation.

Data Analysis

EMG signals were recorded using a unit gain amplifier headstage (Digitimer, NL100) connected to a Neurolog amplifier (x 1000 amplification; Digitimer,NL 900D). Signals were bandpass filtered between 50Hz and 10000 Hz and digitised using an analog to digital interface (1401micro, CED, Cambridge,UK) and the data stored on a PC. The data was visualised using Spike2 software (CED, Cambridge, UK) running on the PC, where the data was saved for offline analysis. Raw traces were analysed using Signal 2.7 (CED, Cambridge, UK). Signal 2.7 was used to generate the H reflex trace averages (n=15) at each threshold/interval. Latencies were measured as peak to peak and amplitudes as the absolute maximum of the averaged traces. H waves were always normalised to either M max or the amplitude of the averaged control H wave (15 averaged waves).

Surgical Procedures

Spinal cord transection

In order to assess the development of spinal circuits in the absence of descending input, neonatal (PN5) spinal cord transections were performed. To correctly determine litter age with an accuracy of ± 3 hours, pregnant mothers were checked 3 times per day from gestational day 19 (E19) until the litter was born. Litters born overnight were not used as there could be error of up to 12 hours. The day of birth was called postnatal day 0 (PN0) and all transections took place at PN5.

All the pups were separated from the mother immediately prior to surgery. Pups were washed thoroughly with saline and then deeply anaesthetised (loss of paw withdrawal) using isoflurane (4% induction, maintained at 1.5%). Upon loss of withdrawal reflex, pups were subcutaneously injected with warm saline (37℃, 200µl) and a midline, dorsal incision was made to the skin near the base of the scapulae. The paravertebral muscles were retracted laterally to reveal the mid-thoracic vertebral laminae. A mid thoracic (T8-10) laminectomy was performed and the cord and meninges were completely severed using micro-scissors. Completion of the transection was ensured by observing the base of the vertebral canal and complete separation of the two distal stumps of the spinal cord. Post mortem histological examination of the injury confirmed completeness. A piece of Gelfoam® was then inserted into the cavity and the wound was closed with silk sutures. Buprenorphine was administered at 0.1mg/kg before the pups regained consciousness to relieve pain. Pups were placed in an incubator to recover fully before being returned to the mother.

Cholera toxin β injections

During the same surgery, cholera toxin β (7.5mg/ml) was pressure injected into the gastrocnemius muscle using a glass micropipette attached to a Hamilton syringe. A small incision was made over the medial gastrocnemius muscle, the needle was inserted and 1 µl was slowly injected. The needle was left in the muscle for 5 minutes and retracted very slowly to prevent leakage.

Immunohistochemistry

Tissue Processing

Following H reflex recordings, preparations were moved to a fume hood perfusion circuit and transcardially perfused with 4% paraformaldehyde in 0.1M phosphate buffer. Vertebral columns containing the spinal cords of animals were harvested and post fixed overnight (4% PFA). Spinal cords were dissected out of the bony encasing and cryoprotected in sucrose (30% in PBS) for at least 48 hours. Segments T13-S1 of the spinal cord were individually separated and frozen in optimal cutting temperature compound (OCT, Leica). A cryostat (1850, Leica Biosystems) was then used to cut transverse serial sections (25µm) of L4-5 which were used for all analyses in this study.

All Immunohistochemical staining was conducted using the same principle steps. Free floating sections were washed in phosphate buffered saline (PBS, 3 x 10 minutes) and then blocked in 3% normal donkey serum and phosphate buffer (0.01M) with 0.2% Triton X-100 (PBST) for 1 hour before being incubated overnight in primary antibodies (Table 1) for 24-48 hours. Sections were then incubated in secondary antibodies which had been raised primarily in donkey and against the immunoglobulin (IgG) in which the primary antibody had been raised. The secondary antibodies were conjugated to Alexa 488 or 555 and biotinylated antibodies were revealed using avidin-Pacific Blue

(Invitrogen). All antibodies were diluted in blocking solution (same concentrations as blocking step).

Imaging and Analysis of IHC data

Confocal Imaging and quantification of boutons

All images were taken using a confocal LSM 700 at 63x (oil immersion). The same microscope was used for the entirety of any experiment. For most analyses the pinhole was adjusted to 1µm optical slices and images were taken as close to the centre of the cell as possible (nucleus visible). All motoneurons on triplicate sections from L4-5 were imaged per animal. All stated ‘n’ relate to animal numbers. Synaptic boutons were only included if they were in close apposition to the neurone and the count was normalized to100µm of the neuron perimeter. Tile scans of whole sections were taken at 20x magnification through 1 confocal plane and all sections were imaged using the same settings. For quantification of lamina distribution of VGLUT1, 2 regions of interest (ROI) were defined: dorsal (ROI^{d}) and intermediate (ROI^{i}). To account for changes in size of the spinal cord sections with age, the ROIs were normalised to the size of the section based on anatomical landmarks. The dorsal ROI box dimensions were normalised by: height-25% of the length of a straight line from base of dorsal column to cord dorsum, width-20% of horizontal line from base of dorsal column laterally to termination of grey matter. The intermediate ROI was the height of the central canal and extended from the lateral edge of the central canal to the lateral termination of the grey matter. Image J particle analysis was used to quantify the density of $VGLUT1^{+}$ terminations in the defined regions. First, images were converted to binary and a minimum bouton diameter of 2µm was defined as the threshold (Ichiyama et al., 2006). All measurements of

density were expressed as percentage coverage of the total area of the ROI analysed. Motoneurons selected for analysis of synaptic coverage were chosen based on size. All motoneurons were imaged, but only cells with a diameter greater than 25μm were analysed as γMNs tend to be under 20μm in diameter (Ichiyama et al., 2006).

Z stacks and 3D reconstruction

In some cases, it was necessary to use Z stack images in order to analyse cells which received very few contacts, or if the contacts were mainly distributed on dendrites (Mentis et al., 2006). This protocol was also used for quantification of axo-axonic presynaptic contacts because it is impossible to reliably identify the centre of the VGLUT1$^+$ terminal in the z plane. In these cases, 0.5μm steps were used with a 63x lens through the entirety of the cell and its dendrites. Images were reconstructed using Imaris 8.1 (Bitplane) and 3D rendered cells were used to quantify surface area and verify terminal contact.

Analyses of VGLUT1$^+$ contacts on RCs

For at least 3 animals per group, RC from 3 free floating sections were analysed. Total cell numbers per group were: Intact- PN10= 72, PN14= 59, PN21= 56, PN5TX-PN10=74, PN14= 55, PN21= 62. The length of the dendrites analysed was the first 50μm for every cell. 3D reconstructions were quantified by normalising VGLUT1$^+$ contacts to RC surface area (number of VGLUT1 boutons/100 μm^2).

Analyses of P bouton contacts on VGLUT1$^+$ PA

3D reconstructions were quantified by normalising number of P boutons to VGLUT1$^+$ PA surface area (number of P boutons/10 µm^2). P bouton contacts were only quantified on VGLUT1$^+$ PA that were closely apposed to ChAT$^+$ MNs. There were at least 3 animals per group, with 3 free floating sections analysed per animal. The total number of VGLUT1$^+$ PA on which P boutons were quantified were: Intact- PN10= 572, PN14= 500, PN21= 474, PN5TX-PN10= 400, PN14= 483, PN21= 463.

1.1 Statistics

All statistical tests were performed using IBM SPSS 22 statistics package. Tests for normal distribution of data were performed before comparisons were made. In cases where the data were normally distributed, univariate analysis of variance tests were performed with Bonferroni post hoc for pairwise comparisons. For data that were not normally distributed, Kruskal-Wallis tests were used with Bonferroni corrections performed on multiple comparisons produced by Dunns tests. For comparing Hmax/Mmax or threshold values between intact and PN5TX at PN14 only, Mann-Whitney U tests were performed.

Results

To create a longitudinal profile of sensorimotor circuit development, we targeted ages PN10, 14 and 21. At PN10 motor control in rats is immature. PN14 marks a dramatic transition to near mature motor control and at PN21 the motor system is considered largely indistinguishable from adult rats.

Normal development of proprioceptive afferents in the presence and absence of descending systems

In the cervical spinal cord, proprioceptive afferents (PA) and descending systems develop in an activity-dependent, competitive manner. The cervical cord is functionally distinct from the lumbar cord of the rat in that the forelimbs are used for skilled tasks (grasping and manipulation) as well as locomotion. Reaching and grasping involves fine control of small muscles in the forepaws whereas the lumbar spinal circuitry is less associated with such fine control. This led us to investigate whether PA in the lumbar cord develop differently from the cervical cord and if their developmental profile was dependent on the presence of descending systems.

Normal PN development of PA innervation of the lumbar cord.

Using an antibody against vesicular glutamate transporter 1 (VGLUT1) to identify PA, density of terminals was assessed in dorsal and intermediate regions of interest in the spinal cord, as well as directly onto MNs. Results showed reduced VGLUT1^{+} terminal density in dorsal, intermediate and ventral regions (MNs) of the spinal cord between PN10 and 14, however in most cases there was little change between PN14 and 21. In the dorsal horn there was a significant effect of development on PA termination densities ($p= 0.008$, Figure 4H). Densities were significantly greater in PN10 animals (63.64 ± 1.46%, n=3) compared to PN14 (39.11 ± 3.76%, $p=0.012$, n=4,) and PN21 (42.31 ± 5.27%, $p=0.023$, n=5, Figure 4H) but there was no difference between PN14 and 21 ($p=.830$), suggesting development of these inputs ceases at this stage. In the intermediate region, there was also a significant effect of age on VGLUT1^{+} terminal density ($p=0.020$, Figure 4I). Similar to the dorsal horn, there was a reduction in VGLUT1^{+} terminal density between PN10 (14.31 ± 3.32%) and PN14 (3.78 ± 0.70%, $p=0.029$) and PN21 (5.59 ± 0.65, $p=0.049$) but there was

no difference between PN14 and PN21 (p=0.803). We appreciate that in the dorsal and intermediate grey, VGLUT1$^+$ boutons are also sourced from the CST and low threshold mechanosensory fibres, which both undergo significant postnatal changes (Varoqui et al., 2002; Todd et al., 2003; Fitzgerald, 2005; Martin, 2005; Du Beau et al., 2012). However, in contrast to both proprioceptive and cutaneous afferents, CST axons proliferate in the lumbar grey between PN10 and 14, indicating that reduced VGLUT1$^+$ bouton density in dorsal and intermediate regions is solely due to afferent retraction, and most likely underestimated (Donatelle, 1977; Joosten et al., 1989).

In the ventral horn, there was a significant effect of age (p=0.005) on VGLUT1$^+$ terminal density in close apposition with MNs (Figure 4J). At PN10 (4.51 ± 0.24 boutons/100µm soma perimeter, n= 3, Figure 4E) the density of VGLUT1$^+$ boutons on MNs were greater than at PN14 (3.46 ± 0.26, p= 0.031, n=3, Figure 4F) and PN21 (3.1 ± 0.26, p= 0.006, n=3, Figure 4G), however there was no difference between PN14 and 21 (p=0 .632).

Neonatal transection prevents retraction of proprioceptive afferents in the lumbar spinal cord.

Following PN5TX, retraction of VGLUT1$^+$ terminals observed during normal development was completely abolished. In dorsal and intermediate regions, CST axons and cutaneous afferents are also VGLUT1$^+$(Alvarez et al., 2004; Du Beau et al., 2012). Considering that CST is absent following TX and the only other sources of this VGLUT1 are proprioceptive and cutaneous afferents, we can conclude that developmental retraction of afferents is abolished in the absence of descending systems. In the dorsal region, there was no difference between intact and TX groups at PN10 (Intact= 63.64 ± 1.46, TX= 67.33 ± 6.63,

p=.512, n=3, Figure 4B & B') however at both PN14 (Intact= 39.10 ± 3.75, TX= 51.23 ± 2.10, p=0.030, n=3, Figure 4C & C') and PN21 (Intact= 42.32 ± 5.27, TX= 60.88 ± 1.46, p=0.030, n=3, Figure 4D & D') transected groups had greater densities of VGLUT1$^+$ puncta (Figure 4H). For intermediate regions (Figure 4I), again the normal developmental trend was abolished for VGLUT1$^+$ boutons (p=0.356). There was no difference between groups at PN10 either (intact= 14.31 ± 3.32, TX= 7.88 ± 5.02, p=0.645). At PN14 there was also no difference between intact and TX groups (intact= 3.78 ± 0.70, TX= 9.67 ± 1.26, p=0.060). At PN21 neonatal TX resulted in a greater density of VGLUT1 puncta (intact= 5.59 ± 0.65, TX= 14.33 ± 0.34, p= 0.010).

On MNs, significant retraction of PA boutons during normal development was abolished by PN5TX (p=.514, Figure 4E-G' & J). At PN10 VGLUT1$^+$ puncta densities were not different between groups (Intact= 4.508 ± 0.25, TX= 4.53 ± 0.44, p= .966, n=3, Figure 4E-E'), however TX groups had greater densities at both PN14 (Intact= 3.46 ± 0.28, TX= 4.99 ± 0.44, p= 0.009, n=3, Figure 4F-F') and PN21 (Intact= 3.14 ± 0.28, TX= 4.18 ± 0.36, p= 0.034, n=3, Figure 4G-G').

Descending systems are necessary for retraction of PA from Renshaw cells

A lack of normal retraction of afferents from dorsal and intermediate zones as well as MNs suggests that interneuron populations may also be affected by PN5TX. In order to test this, we assessed VGLUT1$^+$ terminal density on Renshaw cells, which reportedly originate exclusively from PA afferents (Mentis et al., 2006).

PA terminals are retracted from RCs during PN development

Antibodies against Calbindin D-28k revealed Renshaw cells and extensive portions of their proximal dendrites in the ventral horn of the lumbar spinal cord (Figure 5A-A''). Because PA terminals on RCs are sparse, and mainly distributed on their dendritic processes, 3D reconstructions of Calbindin^{+} RCs and PA boutons were used to quantify terminals contacting the soma and dendrites (Figure 5A-B''). During normal development, there was a significant retraction of PA terminals from RCs ($p= 0.014$). This was true for the soma ($p= 0.004$, Figure 5F), dendrites ($p= 0.003$) and cell overall ($p= 0.05$). For the whole cell (soma and dendrites combined), there was a reduction in PA terminations on RCs between PN10 (1.21 ± 0.06 per $100\mu m^2$, $n=3$) and PN14 (0.68 ± 0.15, $n=3$, $p= 0.011$) and PN10 and PN21 (0.63 ± 0.11, $n=3$, $p= 0.008$), however this reduction in PA afferent input plateaus at PN14 as there was no significant difference between PN14 and 21 ($p= 0.76$). On the soma, there was a significant difference between PN10 (0.72 ± 0.02) and PN14 (0.52 ± 0.09, $p= 0.043$) and PN21 (0.27 ± 0.02, $p= 0.001$). Additionally, there was a decrease between PN14 and 21 ($p= 0.022$). For the dendrites, we saw a significant reduction in PA contacts between PN10 (1.92 ± 0.08) and PN14 ($1.17 \pm .14$, $p= 0.002$) and PN21 (1.15 ± 0.06, $p= 0.002$), however there was no difference between PN14 and 21 ($p= 0.94$).

Disrupted development of PA boutons on RCs following neonatal transection

In the PN5TX group, there was no effect of age on PN development of PA terminals contacting RCs ($p= 0.144$), suggesting development was significantly disrupted. The effect of age was abolished on the soma, and there were no significant differences between intact and TX groups at any of the ages

compared (PN10 intact= 0.716 ± 0.02 per 100µm^2, TX= 0.66 ± 0.12, n= 3, p= 0.62, PN14 intact= 0.52 ± 0.09, TX= 0.76 ± 0.06, n= 3, p= 0.057 and PN21 intact= 0.27 ± 0.02, TX= 0.43 ± 0.11, p=0.213, n=3, Figure 5F). On the proximal dendrites of RCs, again PN5TX acted to disrupt retraction of PA. When each time point was considered, intact and TX groups were not statistically different at PN10 (intact= 1.92 ± 0.08 per 100µm^2, TX= 1.85 ± 0.27, p= 0.768, Figure 5G) and PN21 (intact= 1.15 ± 0.07, TX= 1.23 ± 0.27, p= 0.774) but the TX group had greater PA puncta density at PN14 (intact= 1.17 ± 0.14, TX= 1.80 ± 0.08, p= 0.027, Figure 5D-D', G). When values for dendrites and soma were combined to evaluate the whole cell, again development was shown to be significantly disrupted (p= 0.063). There was no significant difference between intact and TX groups at PN10 (intact= 1.21 ± 0.07 per 100µm^2, TX= 1.07 ± 0.10, p=.454) or PN21 (intact= 0.63 ± 0.10, TX= 0.92 ± 0.05, p=.454) but at PN14 the transection group had a greater density of PA boutons apposing Renshaw cells (intact= 0.67 ± 0.15, TX= 1.36 ± 0.16, p= 0.002). Therefore, we show that PN5TX disrupts development of PA inputs to RCs due to significantly greater density at PN14.

Neonatal transection disrupts the normal formation of motor axon collaterals on Renshaw cells.

Motor axon collaterals provide excitatory drive to adult RCs in a recurrent inhibition circuit exhibiting remarkable efficacy (Moore et al., 2015). Because of the lack of PA retraction following PN5TX shown above, we wanted to assess if this had any bearing on the development of motor axon inputs to RCs. This was done by quantifying VAChT$^+$ boutons on RCs (Figure 6A-E) throughout development in the presence and absence of descending systems.

Intact animals did not exhibit a significant effect of age on RC VAChT$^+$ terminals, suggesting that these remained relatively stable throughout development (Figure 6E). In the PN5TX group, there was a significant effect of age ($p= 0.005$) suggesting that PN5TX significantly altered the developmental profile. Comparisons of values for the two groups at each age revealed no significant differences at PN10 (Intact= 3.86 ± 0.64 per 100µm soma perimeter, n=3 TX= 3.94 ± 0.33, n=3) or 14 (Intact= 4.50 ± 0.82, n=3,TX= 4.45 ± 0.12, n=3, $p= 0.954$) however there were significantly fewer VAChT$^+$ boutons on RCs from PN5TX spinal cords at PN21(intact= 4.77 ± 0.38, n=3, TX= 2.78 ± 0.18, n=3, $p= 0.013$).

In summary, it is likely that the lack of PA retraction following PN5TX results in a subsequent decrease in motor axon synapses (Figure 6F-F').

Postnatal development of GABApre projections to PA terminals in the presence and absence of descending systems.

Proprioceptive afferent activity is heavily modulated by axo-axonic contacts (P boutons) from GABApre neurons, via presynaptic inhibition (PAD) (Hughes et al., 2005; Rudomin, 2009). It has recently been suggested that differentiation of GABApre projections depend upon availability of target PA terminal and local glutamate signalling (Betley et al., 2009; Mende et al., 2016). The extreme developmental retraction of PA and lack thereof following PN5TX provided a unique assay to characterise the developmental profile of GABApre projections and their dependence on both sensory and descending inputs. GAD65$^+$ boutons contacting PA terminals, which directly apposed MNs were quantified using 3D IMARIS reconstructions. All PA terminals contacting MNs were analysed (Figure 7A-B'').

GABApre projections (P boutons) proliferate as PA terminals are retracted in normal development.

We found that while PA were retracted with normal development, the density of P boutons on PA terminals significantly increased with age ($p = 0.0001$, Figure 7I). Interestingly, this increase occurred between PN10 (0.45 ± 0.05, n=3, Fig 7C-C'') and PN14 (1.04 ± 0.03, n=3, $p = 0.0001$, Figure 7D-D'') with it reaching its maximal limits between PN14 and PN21 (1.04 ± 0.03, n=3, $p=0.997$, Fig 7E-E''), when the PA retraction is maximal. PN10 and 21 were also significantly different from each other ($p= 0.0001$). At PN10, 41.61 % (± 2.65) of Ia boutons directly apposing MNs were devoid of P boutons; this was reduced to 11.72% (± 1.91) at PN14 ($p= 0.0001$) and 6.37% (± 0.14) at PN21 ($p= 0.0001$, Figure 7K). There was a concomitant increase ($p<0.0001$) in the quantity of GABApre clusters on PA terminals containing 3 or more P boutons (3+ clusters, Figure 7J) between PN10 (7.86 ± 0.89) and PN14 (38.84 ± 3.99, $p= 0.0001$) and PN21 (44.47 ± 3.44, $p= 0.0001$) but again there was no change between PN14 and 21 ($p= 0.06$). If PA terminal surface area was substantially increased with age, it could be argued that younger animals have less available space for P boutons to contact and this could be responsible for reduced 3+ clusters at PN10. Our analysis showed that there was no change in Ia afferent terminal surface area between PN10 (intact-21.77 ± 0.89 µm, TX-20.68 ± 1.54 µm) and PN14 (intact-22.80 ± 0.66 µm, TX-22.81 ± 1.04 µm) however, there was an increase between PN10 and PN21 (intact 26.54 ± 0.57 µm, $p= 0.006$, TX-24.90 ± 0.85 µm, $p=0.03$). There was no difference between intact and TX groups at any age**.**

Neonatal transection significantly attenuates proliferation of GABApre projections to PA terminals

The results above show that during normal development, GABApre projections proliferate as Ia afferents are retracted. Because PA terminal density is increased following PN5TX, we assessed the impact this had on P bouton density.

We found no difference in quantity of P boutons closely apposing PA terminals between intact and PN5TX animals at PN10 (intact= 0.45 ± 0.048, TX= 0.36 ± 0.032, n=3, p= 0.255, Figure 7C-F''), just as we saw no difference in PA density at this stage**.** In contrast, there were significantly fewer P boutons in the TX group at PN14 (intact= 1.04 ± 0.03, TX= 0.56 ± 0.02, n=3, p= 0.001, Figure 7D-G'') and PN21 (intact= 1.04 ± 0.03, TX= 0.75 ± 0.12, n=3, p= 0.004, Figure 7E-H''). This was due to a greater proportion of PA terminals devoid of P boutons at PN14 (intact= 11.79 ± 1.95%, TX= 33.36 ± 1.42%, p= 0.002) and PN21 (intact=6.37 ± 0.14%, TX=23.61 ± 6.91 %, p= 0.008). Similarly, PA terminals apposed by clusters of >3 P boutons were also reduced at these ages (PN14- intact= 38.84 ± 3.99%, TX= 18.10 ± 1.03%, p= 0.001, PN21- intact= 44.47 ± 3.45%, TX= 27.61 ± 4.22%, p= 0.001). It is important to note however, that despite this attenuation there was still a significant increase in P bouton density in the PN5 TX group between PN10 and 21 (PN10-0.36 ± 0.03, PN21-0.75 ± 0.12, p= 0.001).

In summary, our analyses show that as PA terminals are retracted during normal development, GABApre projections proliferate. This profile is severely, but not completely attenuated by PN5TX (Figure 8).

Hyper-excitability of the monosynaptic reflex following neonatal transection.

Our anatomical data shows reduced retraction of afferents, reduced modulatory input from GABApre neurons and reduced motor axon input to RCs, collectively

548 suggesting that development in the absence of descending systems induces
549 hyper-excitability of the lumbar sensorimotor circuitry. We tested this
550 hypothesis by assessing H reflexes in a perfused whole rat preparation which is
551 viable throughout PN development (first described by Pickering and Paton
552 (2006)). The development of this preparation was vital to the success of these
553 experiments. The decerebration was necessary to negate the variable effects
554 of anaesthetics, such as ketamine on the developing CNS. Additionally, the low
555 blood volume of neonates means haemorrhaging upon severance of major
556 vessels (as occurs with decerebration) leads rapidly to hypovolaemic death.
557 Our perfused preparation allowed full control of the systemic volume, pressure
558 and oxygenation levels and as a result, greater success rates without the need
559 for anaesthesia.
560 Interestingly, we were not able to evoke H reflexes at PN10. H reflexes were
561 also absent at this age in ketamine anaesthetised rats (data not shown). H
562 reflex amplitudes, thresholds and interactions did not vary greatly between
563 PN14 and 21 in intact or TX groups, so these data were pooled. Therefore, H
564 reflexes were assessed between intact and PN5TX rats aged PN14-21.
565 Thresholding revealed that the excitability of the monosynaptic reflex was
566 increased in PN5TX animals due to lower thresholds for evoking H reflex
567 responses (intact = 37.3 ± 6.6 mA, n=6, TX=23.9 ± 3.2 mA, p= 0.050, n=7,
568 Figure 9A). Similarly, PN5TX resulted in a significantly greater Hmax/Mmax
569 ratio (intact= 0.25 ± 0.04 mV, n=5, TX= 0.39 ± 3.21 mV, n=4, p= 0.046, Figure
570 9B). There were no significant differences between groups in H reflex latency.
571 For assessing homonymous paired pulse inhibition between groups we used 7
572 inter-pulse intervals from 700-1ms. The evoked H reflex response was
573 extremely low at intervals between 10 and 1 ms, presumably due to axonal

collisions. There were significant differences, however, at intervals 700 to 50 ms and an overall effect of PN5TX on paired pulse depression. At each time interval, PN5TX animals displayed significantly attenuated PPD, resulting in test responses with greater amplitudes represented as a percentage of the control (single pulse) when compared to intact animals (**700ms**-intact= 53.24 ± 2.07%, n=4, TX= 73.47 ± 7.12%, n=3,p= 0.026, **200ms-** intact= 46.80 ± 2.32%, n=6, TX= 74.62 ± 13.33%, n=4, p= 0.001, **50ms**- intact= 29.64 ± 4.14%, n=6, TX=46.81 ± 4.14, n=4, p= 0.040, Figure 9C-D').

Discussion

This study demonstrates that neonatal transection precludes normal development of spinal sensorimotor circuits (Figure 10). We show postnatal retraction of VGLUT1^{+} boutons from dorsal, intermediate, and ventral regions of the lumbar cord, which is completely absent following TX. Importantly, TX also induced malformation of key modulatory microcircuits responsible for presynaptic inhibition of afferents and recurrent inhibition, leading to hyperexcitability of the H reflex in maturity. Therefore, we not only characterise important features of spinal circuit development, but also highlight mechanisms contributing to motor dysfunction in conditions such as cerebral palsy and spinal cord injury.

Developmental retraction of afferents from the lumbar spinal cord is dependent upon the presence of descending systems.

Postnatal development of PA in the cervical spinal cord has been well studied in the rat and cat, but the functionally different lumbar segments have never been assessed. Gibson and Clowry (1999) showed retraction of PA from the ventral horn during development of the rat cervical spinal cord, while

Chakrabarty and Martin (2011a) identified refinement of PA in dorsal and intermediate regions of the cat cervical spinal cord. We show that early postnatally, when locomotion is immature, PA input to lumbar MNs is dense but subsequently retracted as locomotion becomes mature (PN14-21). At the same time points, retraction of VGLUT1^{+} puncta was also seen in dorsal and intermediate regions as well as on RCs**.** It is important to note, however, that Siembab et al. (2016) showed that not all interneuron populations are subject to PA retraction. In addition, development of cutaneous fibres in dorsal and intermediate regions (Fitzgerald, 2005) may have contributed to VGLUT1 retraction.

Our results showing retraction of PA from RC is consistent with previous work demonstrating that PA innervate and activate RCs early postnatally, but inputs in adulthood are greatly reduced and not capable of activation (Renshaw, 1946; Eccles et al., 1957; Mentis et al., 2006).

The mechanisms responsible for afferent pruning during development of the cervical spinal cord are not fully understood, but thought to be related to competition with descending systems (Gibson et al., 2000; Clowry et al., 2004; Martin, 2005; Clowry, 2007; Chakrabarty & Martin, 2011b). An important consideration here is that cervical motor circuits control muscles responsible for reaching and grasping, which require fine control of forelimb muscles and are therefore critically dependent upon interactions between descending and sensory systems (Alstermark & Isa, 2012). The lumbar spinal cord is less associated with fine motor control and therefore may not develop in the same manner. Despite these functional differences between cervical and lumbar cords, we found that lumbar PA development is affected similarly to what has previously been described for cervical PA after altering descending inputs.

Neonatal transection prevents postnatal retraction of proprioceptive afferents.

In contrast to normal development, we show that in PN5TX rats, PA fail to retract. The physiological manifestation of this anatomical finding was reduced H reflex thresholds compared to intact counterparts.

It is appreciated that afferent sprouting in mature spinal cords can be induced by lesions to descending tracts or supraspinal regions (Liu & Chambers, 1958; Nelson & Mendell, 1979; Krenz & Weaver, 1998; Tan et al., 2012). However, the mechanisms leading to increased afferent input following neonatal lesions may be different. Adult injuries are sustained when lumbar spinal circuits are fully mature, having been organised under the influence of both descending and sensory input. When the same injury is sustained neonatally, locomotor circuits are immature and subsequently develop in the presence of sensory input alone. Considering that we show PA retraction during normal development, it is likely that following PN5TX afferents fail to retract rather than sprout. This is consistent with the work of Levinsson et al. (1999) who found that neonatal transection in rats results in immature nociceptive reflexes in adulthood. In this regard, it is reasonable to suggest that descending input to the lumbar cord is necessary for normal development of sensorimotor systems. Indeed, the CST does not innervate the lumbar cord until PN8-9 meaning it has no influence on spinal circuit development in PN5TX rats (Donatelle, 1977). Furthermore, brainstem projections are present in the lumbar cord early PN, but do not mature until the end of the 2nd postnatal week and thus also have little influence on spinal circuit development in PN5TX rats (Bregman, 1987; Vinay et al., 2005). It could be argued that brainstem systems have greater

651 influence on developmental input of PA to ventral motor circuits, as CST lacks
652 direct functional connections here (Alstermark et al., 2004). Indeed, Basaldella
653 et al. (2015) recently showed that genetically reducing vestibular sensation
654 using Nox3 mutant mice lead to greater densities of VGLUT1^{+} boutons on MNs.
655 Alternatively, a lack of retraction may have resulted from homeostatic
656 mechanisms serving to maintain functional levels of excitability following
657 PN5TX. In support of this hypothesis, Mendelsohn et al. (2015) showed that
658 significantly reducing sensory-motor synaptic transmission, without affecting
659 input density, resulted in sprouting of afferent collaterals onto synergistic,
660 heteronymous motoneurons. This, combined with other recent literature
661 suggests that development of PA projection densities is mediated by a
662 combination of activity, positional cues and recognition signals (Sürmeli et al.,
663 2011; Bikoff et al., 2016). However, further work is needed to understand these
664 mechanisms in the context of spasticity in conditions such as CP and SCI.

665 **Neonatal transection disrupts formation of Renshaw cell - motoneuron**
666 **circuit**

667 Renshaw cells powerfully modulate motor output by forming a remarkably
668 efficient recurrent inhibitory circuit with MNs (Bhumbra et al., 2014; Moore et
669 al., 2015). During normal development, both motor axon and PA synapses
670 proliferate on RCs up to PN15, after which PA terminals retract (Mentis et al.,
671 2006a). Siembab et al 2016 recently showed that genetically up or down
672 scaling proprioceptive inputs to RCs significantly regulated the development of
673 motor axon input density. In our study, PA input to RCs was increased as a
674 result of PN5TX. In agreement with Siembab et al (2016), between PN14 and
675 21 motor axon synapses on RCs were severely reduced following TX,
676 suggesting that similar mechanisms are involved. The fact that there was no

677 difference in PA input between intact and PN5TX animals at PN21 suggests
678 that retraction from RCs was restored. Therefore, considering the loss of motor
679 axon input between PN14-21, RCs experience a significant developmental loss
680 of excitatory input following PN5TX, which could be an important determinant of
681 spasticity in our model and CP.

682 **Neonatal transection severely disrupts development of GABApre**
683 **neuron projections.**

684 Accurate control of movement depends on the gating and directing of sensory
685 information in the spinal cord. This control is mediated by GABApre
686 interneurons exerting presynaptic inhibition via axo-axonic projections (P
687 boutons) to sensory terminals (Frank & Fuortes, 1957; Eccles et al., 1961;
688 Hughes et al., 2005; Rudomin, 2009). Neonatal animals often display poorly
689 directed, exaggerated responses to sensory stimuli (Weed, 1917; Stelzner,
690 1971) which are attenuated with PN development, suggesting refinement of
691 afferent projections and/or their modulation. While PN afferent retraction has
692 been demonstrated, development of axo-axonic GABApre contacts on sensory
693 terminals is not understood. In adult cats, Pierce and Mendell (1993) showed
694 that 86% of Ia terminals have P boutons, but it is not known when this profile is
695 established. Betley et al. (2009) demonstrate that GABApre projections express
696 stringent specificity for sensory terminals, shunning MNs even when PA
697 terminations were genetically reduced using $Er81^{-/-}$ mutant mice. Further, the
698 lack of available targets resulted in significant retraction of GABApre
699 projections from the ventral horn. Our data shows co-development of PA
700 terminals and P boutons, with both reaching a plateau with motor maturity
701 (PN14-21). However, P bouton density significantly increased as PA terminals
702 were retracted, showing an inverse rather than direct relationship (Fig 7).

Between PN10 (41.61%) and 21 (6.37%) there was a 35.24% decrease in PA terminals lacking P boutons, indicating that the increase is due to greater GABApre projections to PA, rather than a redistribution of P boutons from retracted PA terminals. This suggests that regulation of GABApre projections cannot be governed solely by local spinal mechanisms. Indeed, adult sacral spinal cord TX also results in P bouton retraction, even though PA terminal density remains unchanged (Kapitza et al., 2012).

Following PN5TX in our study, P boutons apposing PA terminals were severely reduced, but these axo-axonic contacts still proliferated with development. Interestingly, Mende et al (2016) showed that the efficacy of presynaptic inhibition can be regulated by local glutamate and BDNF signalling between sensory terminals and P boutons. Reducing VGLUT1 availability lead to reduced presynaptic inhibition via downregulation of GAD65/67 in GABApre boutons. Given the high PA input and reduced paired pulse depression seen in our study, similar mechanisms may be responsible for the developmental increase in P bouton density despite PN5TX.

Our findings contribute detail and depth towards comprehension of postnatal sensorimotor circuit formation. Although the core locomotor circuitry is functional prenatally, acquisition of mature organisation and therefore behaviour, depends on postnatal integration of descending systems. By removing descending input early postnatally, development of spinal sensorimotor circuits is severely disrupted leading to hyperreflexia. We also identify several features of the sensorimotor circuitry which contribute directly to hyperreflexia. Similar mechanisms have previously been shown to contribute to spasticity in adult injuries, however direct comparisons with neonatal transections will be needed to identify differences and similarities. It is likely

729 that after neonatal injuries, the same circuits contributing to spasticity may also
730 contribute to enhanced functional recovery, thus it is crucial that we target
731 these circuits in order to better understand and treat perinatal and adult lesions
732 to descending systems.

733 Author contributions

734 R.M.I and S.C devised the project and designed experiments. C.C.S designed
735 and performed experiments, including all data collection and analysis. In situ
736 preparation was learned initially at the lab of J.F.R.P, who also provided advice
737 as C.C.S further developed it for this project. C.C.S prepared the manuscript
738 with input from R.M.I, S.C and J.F.R.P.

739

740

741 References

742

743 Alstermark, B. & Isa, T. (2012) Circuits for skilled reaching and grasping.
744 Annual review of neuroscience, **35**, 559-578.

745

746 Alstermark, B., Ogawa, J. & Isa, T. (2004) Lack of monosynaptic
747 corticomotoneuronal EPSPs in rats: disynaptic EPSPs mediated via
748 reticulospinal neurons and polysynaptic EPSPs via segmental
749 interneurons. Journal of neurophysiology, **91**, 1832-1839.

750

751 Altman, J. & Sudarshan, K. (1975) Postnatal development of locomotion in the
752 laboratory rat. Animal behaviour, **23**, 896-920.

753

754 Alvarez, F.J., Villalba, R.M., Zerda, R. & Schneider, S.P. (2004) Vesicular
755 glutamate transporters in the spinal cord, with special reference to
756 sensory primary afferent synapses. Journal of Comparative Neurology,
757 **472**, 257-280.

758

759 Basaldella, E., Takeoka, A., Sigrist, M. & Arber, S. (2015) Multisensory
760 Signaling Shapes Vestibulo-Motor Circuit Specificity. Cell, **163**, 301-312.

761
762 Betley, J.N., Wright, C.V., Kawaguchi, Y., Erdélyi, F., Szabó, G., Jessell, T.M. &
763 Kaltschmidt, J.A. (2009) Stringent specificity in the construction of a
764 GABAergic presynaptic inhibitory circuit. Cell, **139**, 161-174.

765
766 Bhumbra, G.S., Bannatyne, B.A., Watanabe, M., Todd, A.J., Maxwell, D.J. &
767 Beato, M. (2014) The recurrent case for the Renshaw cell. The Journal
768 of Neuroscience, **34**, 12919-12932.

769
770 Bikoff, J.B., Gabitto, M.I., Rivard, A.F., Drobac, E., Machado, T.A., Miri, A.,
771 Brenner-Morton, S., Famojure, E., Diaz, C. & Alvarez, F.J. (2016) Spinal
772 inhibitory interneuron diversity delineates variant motor microcircuits.
773 Cell, **165**, 207-219.

774
775 Bregman, B.S. (1987) Development of serotonin immunoreactivity in the rat
776 spinal cord and its plasticity after neonatal spinal cord lesions.
777 Developmental brain research, **34**, 245-263.

778
779 Brocard, F., Vinay, L. & Clarac, F. (1999) Development of hindlimb postural
780 control during the first postnatal week in the rat. Developmental brain
781 research, **117**, 81-89.

782
783 Bui, T.V., Stifani, N., Akay, T. & Brownstone, R.M. (2016) Spinal microcircuits
784 comprising dI3 interneurons are necessary for motor functional recovery
785 following spinal cord transection. eLife, **5**, e21715.

786
787 Cazalets, J., Menard, I., Cremieux, J. & Clarac, F. (1990) Variability as a
788 characteristic of immature motor systems: an electromyographic study of
789 swimming in the newborn rat. Behavioural brain research, **40**, 215-225.

790
791 Chakrabarty, S. & Martin, J. (2011a) Postnatal refinement of proprioceptive
792 afferents in the cat cervical spinal cord. European Journal of
793 Neuroscience, **33**, 1656-1666.

794
795 Chakrabarty, S. & Martin, J.H. (2011b) Co-development of proprioceptive
796 afferents and the corticospinal tract within the cervical spinal cord.
797 European Journal of Neuroscience, **34**, 682-694.

798

Chen, H.-H., Hippenmeyer, S., Arber, S. & Frank, E. (2003) Development of the monosynaptic stretch reflex circuit. Current opinion in neurobiology, **13**, 96-102.

Clowry, G., Davies, B., Upile, N., Gibson, C. & Bradley, P. (2004) Spinal cord plasticity in response to unilateral inhibition of the rat motor cortex during development: changes to gene expression, muscle afferents and the ipsilateral corticospinal projection. European Journal of Neuroscience, **20**, 2555-2566.

Clowry, G.J. (2007) The dependence of spinal cord development on corticospinal input and its significance in understanding and treating spastic cerebral palsy. Neuroscience & Biobehavioral Reviews, **31**, 1114-1124.

Commissiong, J. & Toffano, G. (1989) Complete spinal cord transection at different postnatal ages: recovery of motor coordination correlated with spinal cord catecholamines. Experimental brain research, **78**, 597-603.

Dietz, V. & Sinkjaer, T. (2007) Spastic movement disorder: impaired reflex function and altered muscle mechanics. The Lancet Neurology, **6**, 725-733.

Donatelle, J.M. (1977) Growth of the corticospinal tract and the development of placing reactions in the postnatal rat. Journal of Comparative Neurology, **175**, 207-231.

Du Beau, A., Shrestha, S.S., Bannatyne, B., Jalicy, S., Linnen, S. & Maxwell, D. (2012) Neurotransmitter phenotypes of descending systems in the rat lumbar spinal cord. Neuroscience, **227**, 67-79.

Eccles, J., Eccles, R.M. & Magni, F. (1961) Central inhibitory action attributable to presynaptic depolarization produced by muscle afferent volleys. The Journal of physiology, **159**, 147-166.

Eccles, J.C., Eccles, R.M. & Lundberg, A. (1957) The convergence of monosynaptic excitatory afferents on to many different species of alpha motoneurones. The Journal of physiology, **137**, 22-50.

Fitzgerald, M. (2005) The development of nociceptive circuits. Nature Reviews Neuroscience, **6**, 507-520.

Frank, K. & Fuortes, M. (Year) Presynaptic and postsynaptic inhibition of monosynaptic reflexes. Vol. 16, Federation Proceedings. FEDERATION AMER SOC EXP BIOL 9650 ROCKVILLE PIKE, BETHESDA, MD 20814-3998, City. p. 39-40.

Fukuhara, K., Imai, F., Ladle, D.R., Katayama, K.-i., Leslie, J.R., Arber, S., Jessell, T.M. & Yoshida, Y. (2013) Specificity of monosynaptic sensory-motor connections imposed by repellent Sema3E-PlexinD1 signaling. Cell reports, **5**, 748-758.

Gao, B. & Ziskind-Conhaim, L. (1995) Development of glycine-and GABA-gated currents in rat spinal motoneurons. Journal of neurophysiology, **74**, 113-121.

Gibson, C.L., Arnott, G.A. & Clowry, G.J. (2000) Plasticity in the rat spinal cord seen in response to lesions to the motor cortex during development but not to lesions in maturity. Experimental neurology, **166**, 422-434.

Gibson, C.L. & Clowry, G.J. (1999) Retraction of muscle afferents from the rat ventral horn during development. Neuroreport, **10**, 231-235.

Hughes, D., Mackie, M., Nagy, G., Riddell, J., Maxwell, D., Szabo, G., Erdelyi, F., Veress, G., Szűcs, P. & Antal, M. (2005) P boutons in lamina IX of the rodent spinal cord express high levels of glutamic acid decarboxylase-65 and originate from cells in deep medial dorsal horn. Proceedings of the National Academy of Sciences of the United States of America, **102**, 9038-9043.

Ichiyama, R.M., Broman, J., Edgerton, V.R. & Havton, L.A. (2006) Ultrastructural synaptic features differ between α-and γ-motoneurons innervating the tibialis anterior muscle in the rat. Journal of Comparative Neurology, **499**, 306-315.

Ichiyama, R.M., Broman, J., Roy, R.R., Zhong, H., Edgerton, V.R. & Havton, L.A. (2011) Locomotor training maintains normal inhibitory influence on both alpha-and gamma-motoneurons after neonatal spinal cord transection. The Journal of neuroscience, **31**, 26-33.

Jean-Xavier, C., Pflieger, J.F., Liabeuf, S. & Vinay, L. (2006) Inhibitory postsynaptic potentials in lumbar motoneurons remain depolarizing after neonatal spinal cord transection in the rat. Journal of neurophysiology, **96**, 2274-2281.

884 Joosten, E., Gribnau, A. & Dederen, P. (1989) Postnatal development of the
885 corticospinal tract in the rat. Anatomy and embryology, **179**, 449-456.

886
887 Kapitza, S., Zörner, B., Weinmann, O., Bolliger, M., Filli, L., Dietz, V. & Schwab,
888 M.E. (2012) Tail spasms in rat spinal cord injury: changes in
889 interneuronal connectivity. Experimental neurology, **236**, 179-189.

890
891 Krenz, N. & Weaver, L. (1998) Sprouting of primary afferent fibers after spinal
892 cord transection in the rat. Neuroscience, **85**, 443-458.

893
894 Kudo, N. & Yamada, T. (1985) Development of the monosynaptic stretch reflex
895 in the rat: an in vitro study. The Journal of physiology, **369**, 127-144.

896
897 Levinsson, A., Luo, X.-L., Holmberg, H. & Schouenborg, J. (1999)
898 Developmental tuning in a spinal nociceptive system: effects of neonatal
899 spinalization. J. Neurosci., **19**, 10397-10403.

900
901 Liu, C.-N. & Chambers, W. (1958) Intraspinal sprouting of dorsal root axons:
902 Development of new collaterals and preterminals following partial
903 denervation of the spinal cord in the cat. AMA Archives of Neurology &
904 Psychiatry, **79**, 46-61.

905
906 Martin, J.H. (2005) The corticospinal system: from development to motor
907 control. The Neuroscientist, **11**, 161-173.

908
909 Mears, S.C. & Frank, E. (1997) Formation of specific monosynaptic
910 connections between muscle spindle afferents and motoneurons in the
911 mouse. The Journal of neuroscience, **17**, 3128-3135.

912
913 Mende, M., Fletcher, E.V., Belluardo, J.L., Pierce, J.P., Bommareddy, P.K.,
914 Weinrich, J.A., Kabir, Z.D., Schierberl, K.C., Pagiazitis, J.G. &
915 Mendelsohn, A.I. (2016) Sensory-Derived Glutamate Regulates
916 Presynaptic Inhibitory Terminals in Mouse Spinal Cord. Neuron.

917
918 Mendelsohn, A.I., Simon, C.M., Abbott, L., Mentis, G.Z. & Jessell, T.M. (2015)
919 Activity regulates the incidence of heteronymous sensory-motor
920 connections. Neuron, **87**, 111-123.

921
922 Mentis, G.Z., Siembab, V.C., Zerda, R., O'Donovan, M.J. & Alvarez, F.J. (2006)
923 Primary afferent synapses on developing and adult Renshaw cells.
924 Journal of Neuroscience, **26**, 13297-13310.

Moore, N.J., Bhumbra, G.S., Foster, J.D. & Beato, M. (2015) Synaptic Connectivity between Renshaw Cells and Motoneurons in the Recurrent Inhibitory Circuit of the Spinal Cord. The Journal of Neuroscience, **35**, 13673-13686.

Nelson, S.G. & Mendell, L.M. (1979) Enhancement in Ia-motoneuron synaptic transmission caudal to chronic spinal cord transection. Journal of neurophysiology, **42**, 642-654.

Ozaki, S., Yamada, T., Iizuka, M., Nishimaru, H. & Kudo, N. (1996) Development of locomotor activity induced by NMDA receptor activation in the lumbar spinal cord of the rat fetus studied in vitro. Developmental brain research, **97**, 118-125.

Petruska, J.C., Ichiyama, R.M., Jindrich, D.L., Crown, E.D., Tansey, K.E., Roy, R.R., Edgerton, V.R. & Mendell, L.M. (2007) Changes in motoneuron properties and synaptic inputs related to step training after spinal cord transection in rats. The Journal of neuroscience, **27**, 4460-4471.

Pickering, A.E. & Paton, J.F.R. (2006) A decerebrate, artificially-perfused in situ preparation of rat: utility for the study of autonomic and nociceptive processing. Journal of neuroscience methods, **155**, 260-271.

Pierce, J.P. & Mendell, L.M. (1993) Quantitative ultrastructure of Ia boutons in the ventral horn: scaling and positional relationships. The Journal of neuroscience, **13**, 4748-4763.

Renshaw, B. (1946) Central effects of centripetal impulses in axons of spinal ventral roots. J Neurophysiol, **9**, 191-204.

Rosenbaum, P., Eliasson, A.-C., Hidecker, M.J.C. & Palisano, R.J. (2014) Classification in Childhood Disability Focusing on Function in the 21st Century. Journal of child neurology, 0883073814533008.

Rudomin, P. (2009) In search of lost presynaptic inhibition. Experimental brain research, **196**, 139-151.

Saunders, N., Kitchener, P., Knott, G., Nicholls, J., Potter, A. & Smith, T. (1998) Development of walking, swimming and neuronal connections after complete spinal cord transection in the neonatal opossum, Monodelphis domestica. The Journal of neuroscience, **18**, 339-355.

Siembab, V.C., Gomez-Perez, L., Rotterman, T.M., Shneider, N.A. & Alvarez, F.J. (2016) Role of primary afferents in the developmental regulation of motor axon synapse numbers on Renshaw cells. Journal of Comparative Neurology.

Stelzner, D.J. (1971) The normal postnatal development of synaptic end-feet in the lumbosacral spinal cord and of responses in the hind limbs of the albino rat. Experimental neurology, **31**, 337-357.

Sürmeli, G., Akay, T., Ippolito, G.C., Tucker, P.W. & Jessell, T.M. (2011) Patterns of spinal sensory-motor connectivity prescribed by a dorsoventral positional template. Cell, **147**, 653-665.

Tan, A.M., Chakrabarty, S., Kimura, H. & Martin, J.H. (2012) Selective Corticospinal Tract Injury in the Rat Induces Primary Afferent Fiber Sprouting in the Spinal Cord and Hyperreflexia. The Journal of neuroscience, **32**, 12896-12908.

Tillakaratne, N.J., Guu, J.J., de Leon, R.D., Bigbee, A.J., London, N., Zhong, H., Ziegler, M., Joynes, R., Roy, R.R. & Edgerton, V.R. (2010) Functional recovery of stepping in rats after a complete neonatal spinal cord transection is not due to regrowth across the lesion site. Neuroscience, **166**, 23-33.

Todd, A., Hughes, D., Polgar, E., Nagy, G., Mackie, M., Ottersen, O. & Maxwell, D. (2003) The expression of vesicular glutamate transporters VGLUT1 and VGLUT2 in neurochemically defined axonal populations in the rat spinal cord with emphasis on the dorsal horn. European Journal of Neuroscience, **17**, 13-27.

Van Hartesveldt, C., Sickles, A.E., Porter, J.D. & Stehouwer, D.J. (1991) L-DOPA-induced air-stepping in developing rats. Developmental Brain Research, **58**, 251-255.

Varoqui, H., Schäfer, M.K.-H., Zhu, H., Weihe, E. & Erickson, J.D. (2002) Identification of the differentiation-associated Na+/PI transporter as a novel vesicular glutamate transporter expressed in a distinct set of glutamatergic synapses. The Journal of neuroscience, **22**, 142-155.

Vinay, L., Ben-Mabrouk, F., Brocard, F., Clarac, F., Jean-Xavier, C., Pearlstein, E. & Pflieger, J.F. (2005) Perinatal development of the motor systems involved in postural control. Neural plasticity, **12**, 131-139.

Weber, E.D. & Stelzner, D.J. (1977) Behavioral effects of spinal cord transection in the developing rat. Brain research, **125**, 241-255.

Weed, L.H. (1917) The reactions of kittens after decerebration. Am. J. Physiol, **43**, 131-157.

Westerga, J. & Gramsbergen, A. (1993a) Changes in the electromyogram of two major hindlimb muscles during locomotor development in the rat. Experimental brain research, **92**, 479-488.

Westerga, J. & Gramsbergen, A. (1993b) Development of locomotion in the rat: the significance of early movements. Early human development, **34**, 89-100.

Figure Legends

Table 1. Antibodies, sources and concentrations.

Figure 1. Preparation set up. (A) Schematic of animal set up with cannulation, recording and stimulation sites shown. Animal is in prone position. (B) Components of the perfusion circuit and flow of ACSF. Red line represents flow from reservoir to preparation and the blue line represents the return flow. 2 pumps are shown for clarity, all tubing actually inserts into a single pump.

Figure 2. Establishing preparation viability. (A) Vasopressin increases systemic pressure leading to higher frequency of respiratory contractions. Red box shows respiratory contractions at low, non-viable pressure, green box indicates high, viable pressure. (B) Shows weak, low frequency respiratory contractions at low pressure. (C) Respiratory frequency markedly increases with increased pressure indicating brainstem viability. (D-E) Motor (EMG) outputs from the left gastrocnemius in response to toe pinch at viable and non-viable systemic pressures.

Figure 3. Stimulation and recording set up. (A-B) shows typical H reflex recruitment curves, demonstrating classical H and M wave responses to increased stimulation strength. (C) Typical H reflex responses to graded stimulation. (D) Experimental setup showing stimulation, recording and axotomy sites. (E) H reflex was confirmed by severing the sciatic nerve at the site marked in (D), resulting in loss of H wave but unaffected M wave.

Figure 4. Postnatal development of VGLUT1$^+$ terminations in the lumbar spinal cord. (A) Typical VGLUT1$^+$ staining with dorsal, intermediate and ventral regions of interest marked. (A') Images were converted to binary for assessment of bouton density in dorsal and intermediate regions of interest. (B-D') Representative heat maps of VGLUT1$^+$ puncta densities at PN10-21 in intact and PN5TX rats. Thresholding is based on maximum and minimum densities. (E-G') Representative images of MNs contacted by PA boutons throughout development in intact and PN5TX rats. (H-J) Quantification of boutons in dorsal (H) and intermediate (I) regions of interest as well as on MNs (J). Scale bars: A=200µm, E=10 µm.

Figure 5. Postnatal development of PA boutons on Renshaw cells. (A-B'') 3D reconstruction of Renshaw cell and PA contacts created using IMARIS software. (C-E') Representative RCs and PA contacts at PN10-21 in intact and PN5 TX rats. (F-H) Quantification of boutons contacting the soma, dendrites and the whole cell for both intact and PN5 TX rats at each age. Scale bars: A''& C =10 µm, B=2 µm

Figure 6. PN development of motor axon collaterals on Renshaw cells. (A-A') Renshaw cells and VAChT^{+} boutons in the ventral horn. (B-D) Calbindin^{+} Renshaw cells contacted by VAChT^{+} motor axon collaterals. (E) Graph showing reduction in motor axon collateral density on RCs between PN14 and 21. (F-F') Schematics illustrating differences between intact and PN5TX rats in development of PA and motor axon inputs to RCs. Scale bars: A=100 µm, E=10 µm

Figure 7. Postnatal development of GABApre projections in intact and PN5TX rats. (A-B'') IMARIS software was used to reconstruct 3D images of PA contacting MNs and associated P boutons. (C-H'') Representative images of P bouton contacts on PA terminals throughout PN development in both groups. (I-K) Quantification of P boutons. (I) Number of P Boutons per 10 µm PA terminal surface area. (J) The percentage of PA terminals with greater than 3 P boutons. (K) Percentage of PA terminals devoid of P boutons. Scale bars: A-A'=5 µm, C= 2µm.

Figure 8. Schematic showing development of GABApre projections (P boutons) and proprioceptive afferents in normal and neonatally transected rats. For intact rats, P boutons increase as afferents are retracted, but there is a lack of PA retraction in PN5TX rats in conjunction with severely attenuated proliferation of P boutons.

Figure 9. Monosynaptic reflex excitability of intact and neonatally transected rats. (A-B) H reflex threshold is reduced and Hmax/Mmax ratio is increased in PN14-21 rats following neonatal transection. (C) Paired pulse depression of the H reflex in intact and neonatally transected rats at PN14-21. Shaded areas highlight the difference in inhibition between intact and PN5TX rats. (D-D') Representative traces from intact and PN5TX rats at long (700 ms) and short (50 ms) time intervals.

Figure 10. Schematic summarising the PN development of the lumbar spinal sensorimotor circuitry in intact and neonatally transected rats. (A) Intact development. (B) Development following neonatal transection.

1102 Figure 1

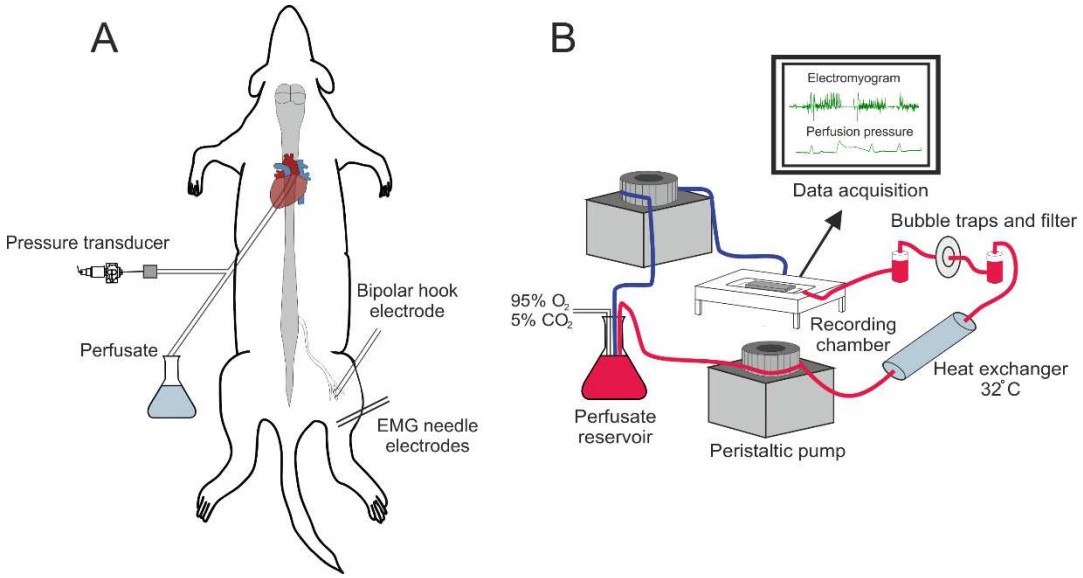

1103

1104

1105

1106

1107

1108

1109

1110

1111

1112

1113

1114

1115

1116

1117

1118

1119

1120 Figure2

1121

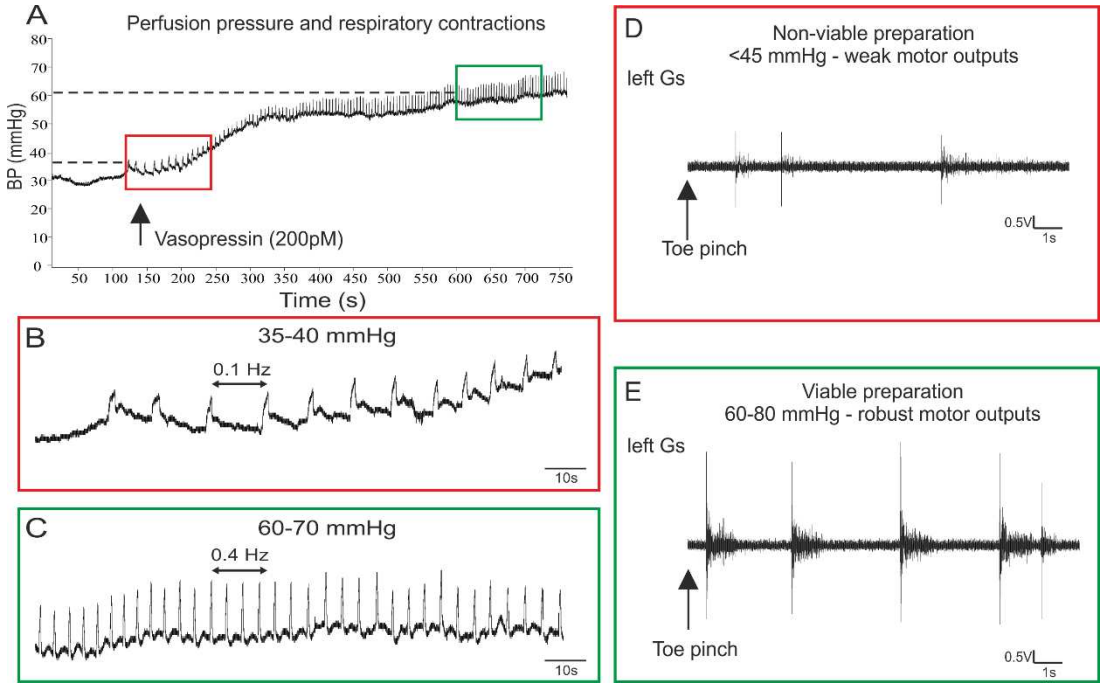

1122

1123 Figure 3

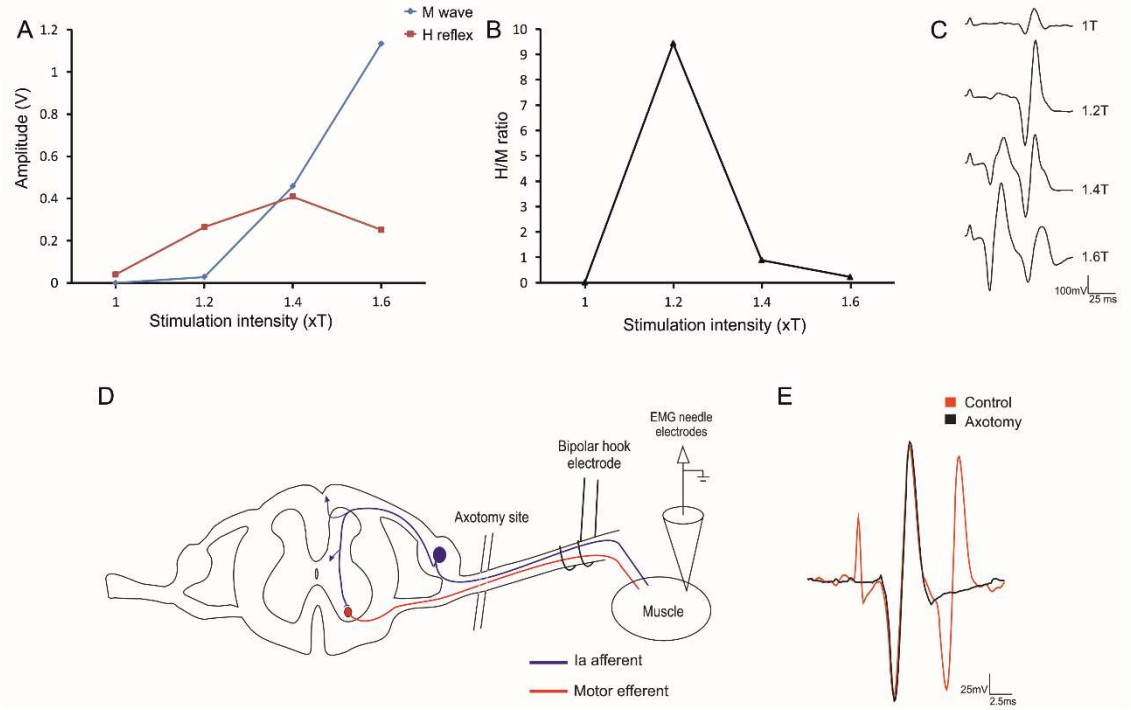

1124

1125

1126

1127

1128

1129

1130 Figure 4

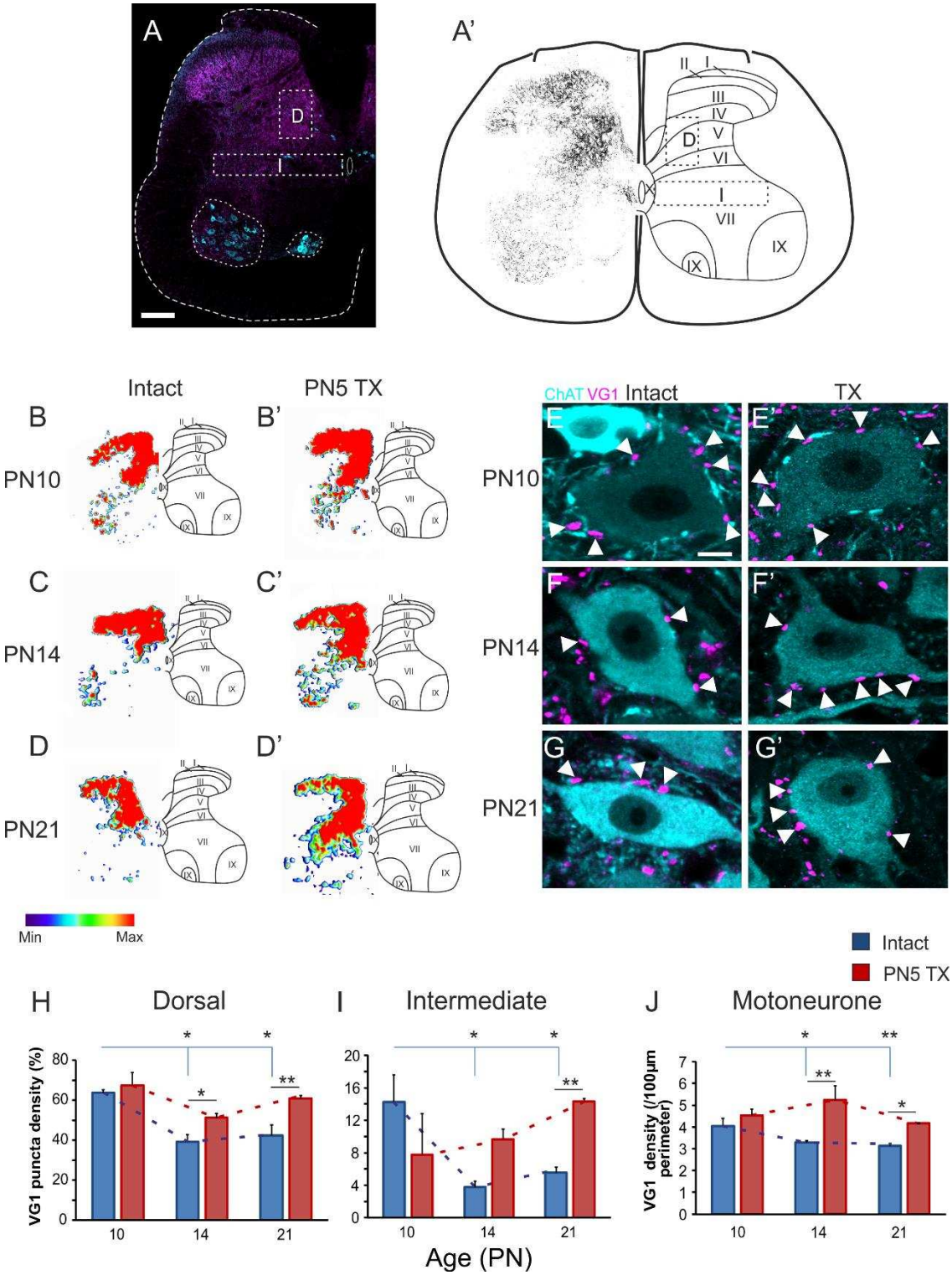

1131

1132 Figure5

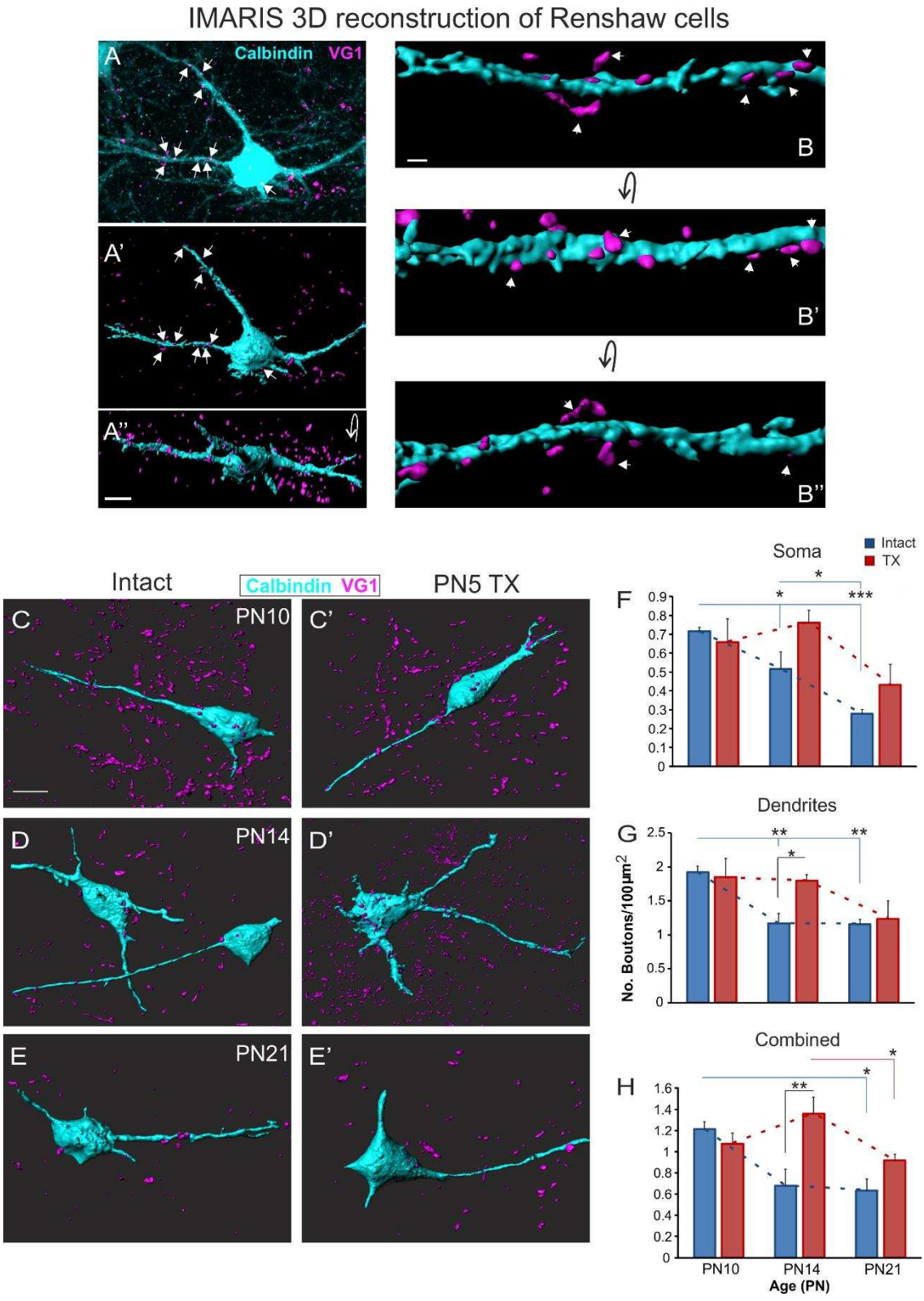

1133

1134 Figure 6

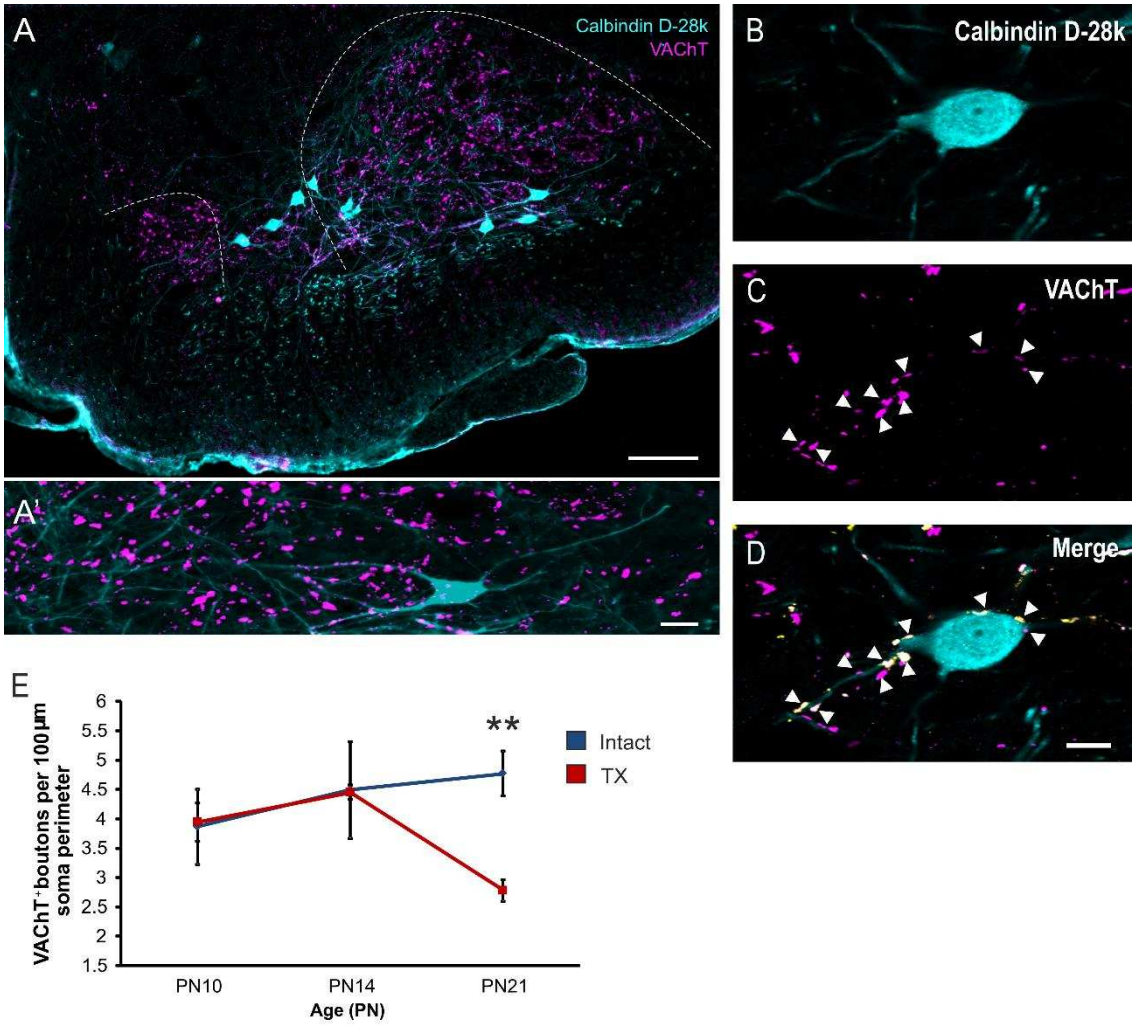

1135

1136 Figure 7

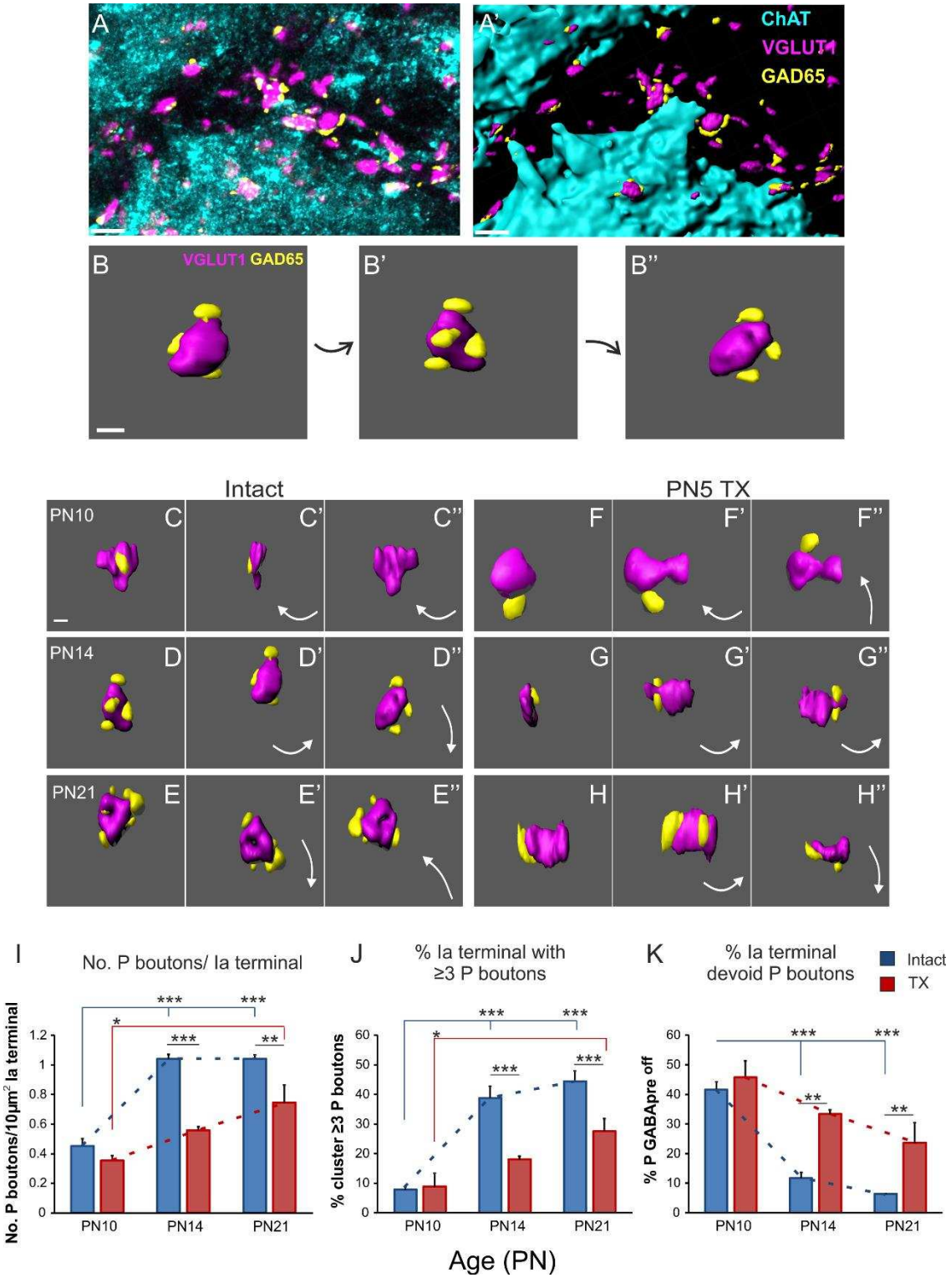

1137

Figure 8

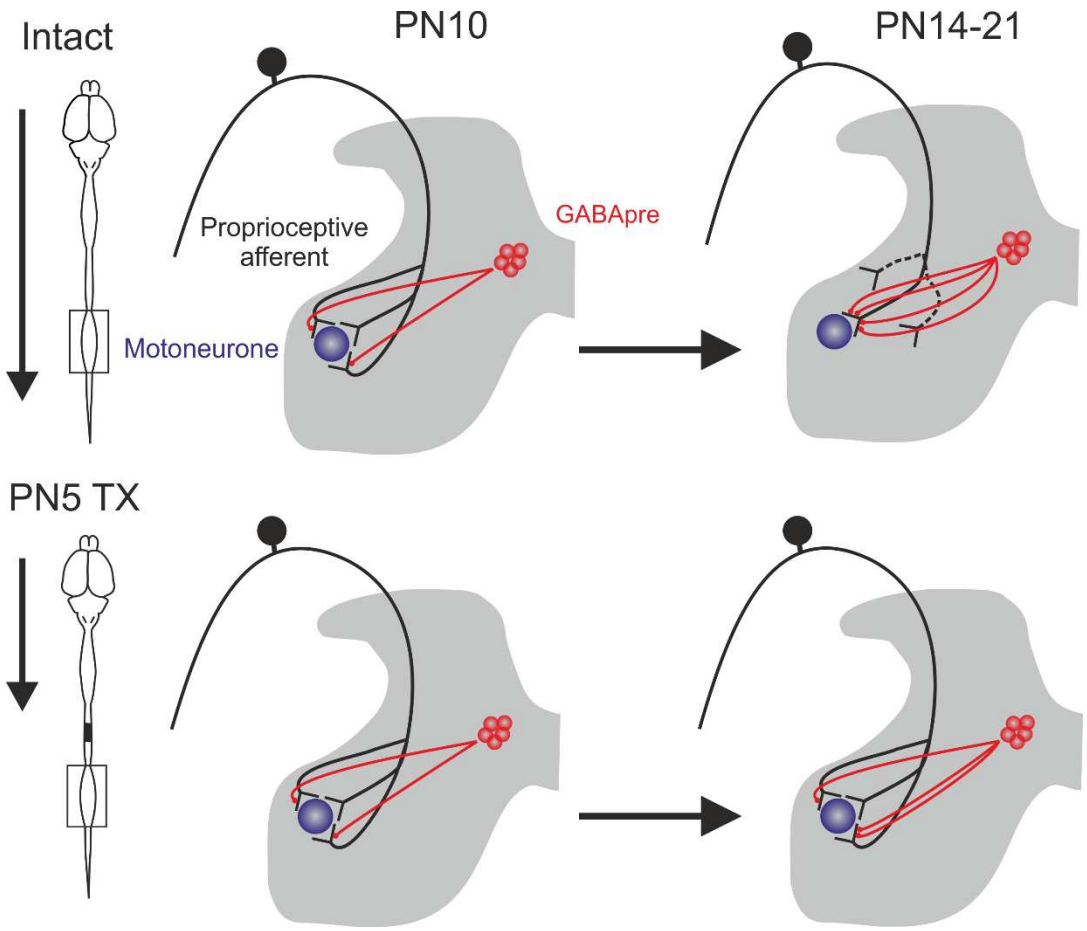
Intact
PN10
PN14-21
Proprioceptive afferent
GABApre
Motoneurone
PN5 TX

1145 Figure 9

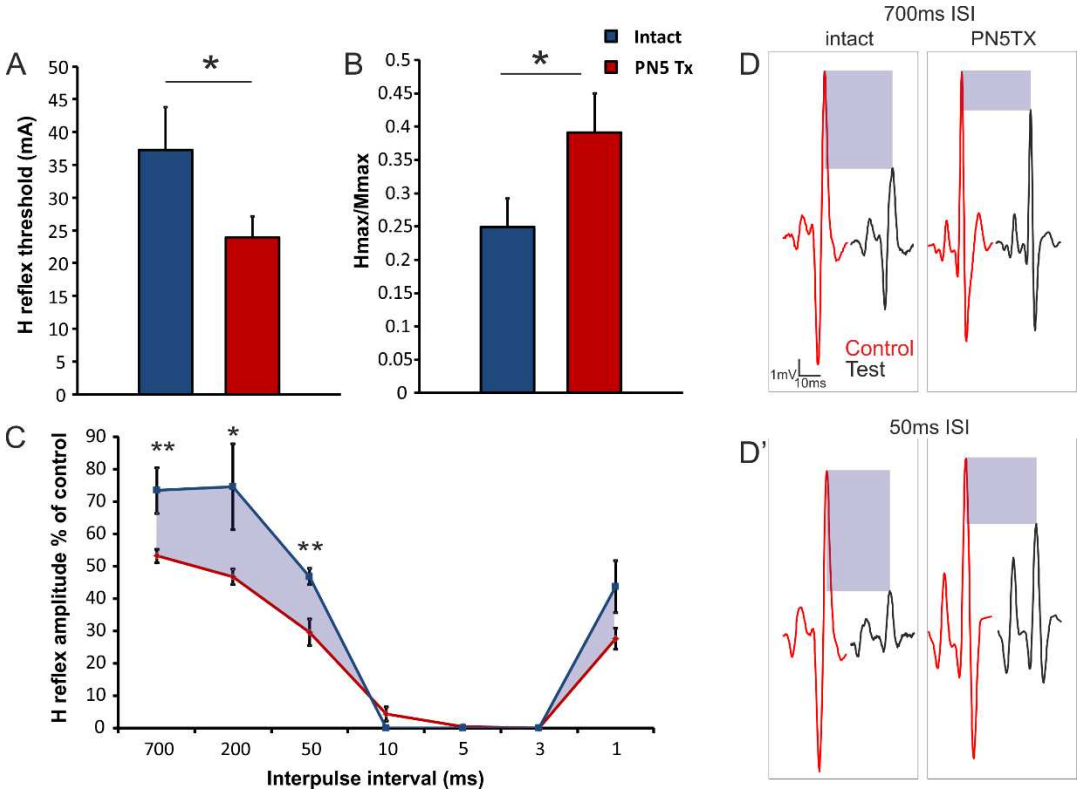

1146

1147 Figure 10

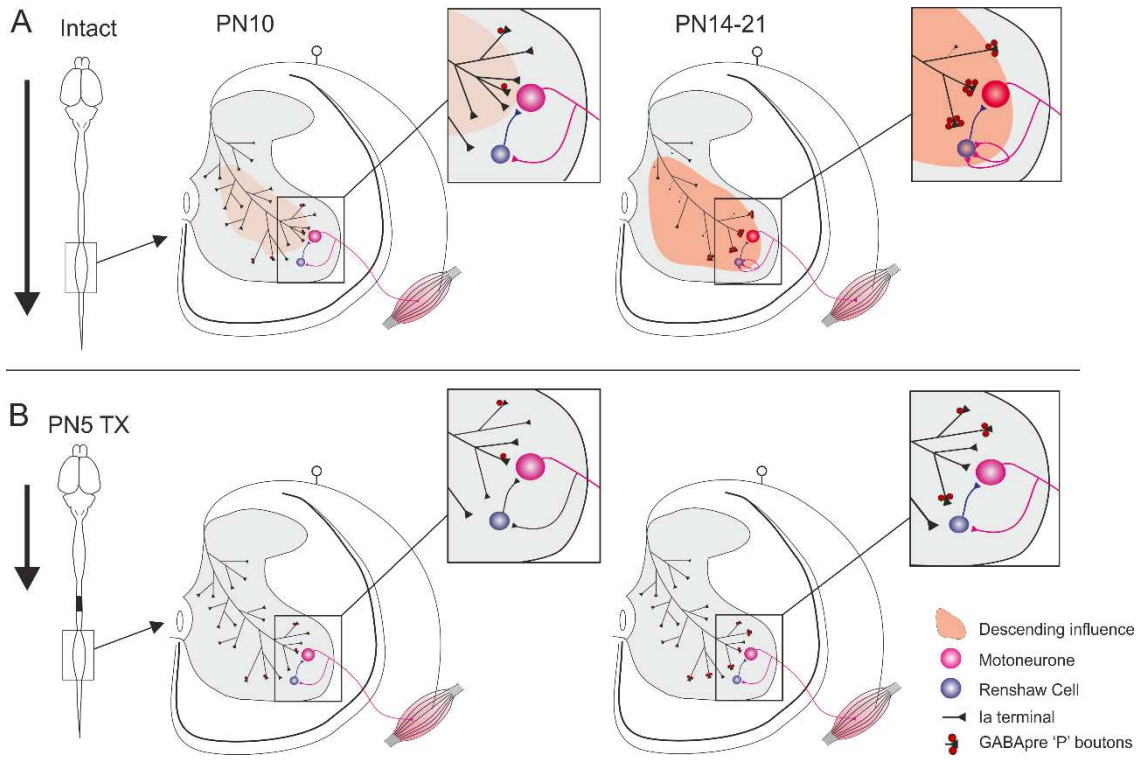

1148